Journal of Power Sources 202 (2012) 190–199

Contents lists available at SciVerse ScienceDirect

Journal of Power Sources

journal homepage: www.elsevier.com/locate/jpowsour

Exploring calcium tantalates and niobates as prospective catalyst supports for water electrolysis

Oleg I. Velikokhatnyi [a], Prashant N. Kumta [a,b,c,d,*]

[a] Department of Bioengineering, University of Pittsburgh, Pittsburgh, PA 15261, United States
[b] Mechanical Engineering and Materials Science Department, University of Pittsburgh, Pittsburgh, PA 15261, United States
[c] Department of Chemical and Petroleum Engineering, University of Pittsburgh, Pittsburgh, PA 15261, United States
[d] Center for Complex Engineered Multifunctional Materials, University of Pittsburgh, Pittsburgh, PA 15261, United States

ARTICLE INFO

Article history:
Received 12 August 2011
Received in revised form 7 November 2011
Accepted 7 November 2011
Available online 15 November 2011

PACS:
71.15.Nc
71.20.Nr
71.20.Ps

Keywords:
Electronic structure
Density functional theory
Calcium niobates
Calcium tantalates
Doping
Catalyst support

ABSTRACT

In an attempt to identify new electrochemically stable catalyst supports for electrolysis of water, the electronic structures of $CaNb_2O_6$, $CaTa_2O_6$, $Ca_2Nb_2O_7$, and $Ca_2Ta_2O_7$ compounds doped with small amounts of elements from 3A, 3B, 5B, and 6A groups of the Periodic table as well as F from group 7B have been calculated using the Vienna *Ab-initio* Simulation Package (VASP), within the projector augmented-wave (PAW) method in the general gradient approximation (GGA) for conducting the exchange-correlation corrections. The role of incorporating the additional elements in improving the electronic conductivity as well as the structural and chemical stability is discussed. Based on the calculated values of the cohesive energies for the materials and their type of electronic conductivity, we hypothesize that group 3A elements (Sc and Y) as well as F-doping contribute drastically to the improvement of the electronic properties as well as the chemical stability of all four calcium tantalates/niobates parent oxides. The study indicates that these doped compounds might therefore serve as the most appropriate candidates for use as catalyst supports in water electrolysis.

1. Introduction

Hydrogen is considered an attractive fuel for transportation and electric grid load balancing [1–4]. The main advantages of hydrogen is its high specific energy, high specific power, low or zero self discharge rates allowing it to be stored for long periods of time unlike the other energy storage media. Further, hydrogen is a cleaner alternative fuel yielding only water as the recyclable by-product resulting in emissions devoid of greenhouse gases and other pollutants compared to the hitherto used known hydrocarbon fuels [1,3]. Thus use of hydrogen as a fuel in proton exchange membrane (PEM) fuel cells to power vehicles and also provide stand alone power to residential and commercial buildings [5–8] in stacked mode offers an attractive solution to the current energy generation, storage, transportation, and distribution gridlock faced by the United States as well as the growing global environmental concerns. The only limitation to achieving this panacea for the global energy storage, generation and distribution problem is the viability of hydrogen fuel aside from its storage, distribution and transportation challenges. As most of the hydrogen on the earth is locked up in water, a conceivably feasible option for producing hydrogen is by electrolysis of water using electricity generated from mechanical energy sources (hydropower or wind turbines).

Advanced water electrolyzers using proton exchange membranes (PEM) generally utilize expensive noble metal electrocatalysts for the oxygen electrode such as platinum and platinum alloys [7] as well as the equally prohibitively expensive iridium oxide (IrO_2) and ruthenium oxide (RuO_2) catalysts. The tremendous costs associated with the use of noble metal oxides at the current loading levels could be substantially lowered by developing new non-noble metal based catalysts that exhibit comparable or improved catalytic activity as the parent noble metal counterparts or identification of electrochemically stable catalyst supports that can be economically synthesized in high surface area (HSA) forms allowing for reduced levels of catalyst loading without compromising the electro-catalytic activity. Thus, it is desirable that these catalyst supports exhibit high electronic conductivity comparable to the noble metals combined with excellent chemical and electrochemical stability at potentials of 1.8–2.0 V against the normal

* Corresponding author at: 3700 O'Hara Street, BEH 849, Pittsburgh, PA 15261, United States. Tel.: +1 412 648 0223; fax: +1 412 624 3699.
E-mail address: pkumta@pitt.edu (P.N. Kumta).

0378-7753/$ – see front matter © 2011 Elsevier B.V. All rights reserved.
doi:10.1016/j.jpowsour.2011.11.022

hydrogen electrode (NHE) wherein electrolysis of water is known to occur.

Very few materials are known to exhibit both the desired electrical conductivity and the much needed electrochemical stability in the 1.8–2.0 V potential window. In this regard, several researchers have proposed [9–13] the use of IrO_2 combined with highly corrosive resistant tantalum oxide (Ta_2O_5), tin oxide (SnO_2), niobium oxide (Nb_2O_5), titanium oxide (TiO_2) and non-stoichiometric tungsten oxide (WO_x) for stabilizing the IrO_2 dimensionally stable anode electrode during the service life of the electrolyzer. However, there is a need to further improve the electronic conductivity to enhance the electro-catalytic activity thus improving the catalyst efficiency and consequently minimizing the catalyst loading.

One approach to achieve this goal would be the introduction of solid solutions of transition metal oxides, such as Nb_2O_5 and Ta_2O_5, with tin oxide, which are known to exhibit the desired high chemical and electrochemical stability but are also well known insulators with poor electronic conductivity. Alloying of the oxides with SnO_2 can likely change their electronic structure, which in turn could positively influence the electronic conductivity. In our recently published first principles theoretical study of different ternary oxides, such as $Sn_2Ta_2O_7$, $Sn_2Nb_2O_7$, $SnTa_2O_6$, and $SnNb_2O_6$ doped with small concentration of elements selected from groups 5B and 6A of the Periodic Table, such as As, Sb, Bi as well as Cr, Mo, and W [14], we had postulated that $SnTa_2O_6$ doped with As, Sb, or Bi would be the most appropriate material for implementation as catalyst supports with respect to all other materials investigated in the study, both in terms of the electronic conductivity as well as structural/chemical stability. Experimental work to explore and validate our reported theoretical predictions is currently on-going in our laboratory. These results will be published shortly.

Besides Sn–Nb/Ta–O oxides there is a large family of bivalent niobates and tantalates (see, for example [15,16]) which remain largely unexplored for possible use as catalyst supports, however their structural and chemical stability is higher than the tin-based oxides. For example, CaO, MgO, and SrO oxides have higher formation enthalpy in comparison to SnO (for ΔH^0 see [17]), thus one can suggest that tantalates and niobates of Ca, Mg or Sr can also be expected to demonstrate higher structural stability than the tin based systems.

The present article is an attempt to offer a range of candidate materials possessing the desired electrochemical stability and superior electronic conductivity compared to tin dioxide as well as tantalum and niobium pentoxides, rendering these materials potentially suitable as possible catalyst supports for water electrolysis and hydrogen fuel cells. Among the materials known to exist in nature and the artificially synthesized niobates and tantalates of different divalent metals, such as Ca, Mg, Sr, Sn, Ba, Zn, Cd, and Pb we chose the most structurally stable system Ca–(Nb or Ta)–O for our investigation. These systems are also known photocatalysts for water splitting and producing hydrogen gas under light illumination [18–20].

Since, all the four $CaNb_2O_6$, $Ca_2Nb_2O_7$, $CaTa_2O_6$, and $Ca_2Ta_2O_7$, are semiconductors it would be interesting to investigate the effect of different dopants selected particularly in light of improving the electronic conductivity necessary for achieving high performance of the potential catalyst supports. These elements would likely serve as donors of additional free electrons participating in the charge transfer and thus, increasing the electronic conductivity. Such elements substituting divalent Ca^{2+} at corresponding sites in the crystal lattice could belong to 3A, 3B, and 5B groups of the Periodic table, while those elements substituting Nb^{5+} and Ta^{5+} in the lattice might belong to 6A group. Also, another likely pathway to donate free electrons into the system is to dope the oxides with small amount of fluorine substituting the corresponding oxygen ions in the crystal structure. An effect of such F-doping could be similar to that observed in fluorine doped tin oxide (FTO) widely investigated experimentally and from first principles also reported by us recently [21–24].

Based on the above, *ab initio* calculations of total energies, electronic and optimized crystal structures, and cohesive energies have been carried out in the present study for the following oxides: $CaNb_2O_6$, $Ca_2Nb_2O_7$, $CaTa_2O_6$, and $Ca_2Ta_2O_7$ in both, pure and doped forms with the introduction of a small amount of 3A group – (Sc, Y), 3B group – (B, Al, Ga, In), 6A group – (Cr, Mo, W), 5B group – (As, Sb, Bi), as well as F. The formula units of the doped materials can be written as: $[Ca_{1-x}(3A, 3B, 5B\ elements)_x][Nb/Ta]_2O_6$, $Ca[(Nb/Ta)_{1-y}(6A\ elements)_y]_2O_6$, $Ca[Nb/Ta]_2O_{6-x}F_x$ and $[Ca_{1-z}(3A, 3B, 5B\ elements)_z]_2[Nb/Ta]_2O_7$, $Ca_2[(Nb/Ta)_{1-z}(6A\ elements)_z]_2O_7$, $Ca_2[Nb/Ta]_2O_{7-x}F_x$, where $x = 0.25$, $y = 0.125$, and $z = 0.0625$.

2. Theoretical approaches and details of the methodology

For calculating the total energies, electronic structure and density of electronic states the Vienna *Ab-initio* Simulation Package (VASP) was used within the projector augmented-wave (PAW) method [25–27] and the generalized gradient approximation (GGA) for the exchange-correlation energy functional in a form suggested by Perdew and Wang [28]. This program calculates the electronic structure and via the Hellmann–Feynman theorem, the inter-atomic forces are determined from first principles. Standard PAW potentials were employed for the elemental constituents of all pure and doped compounds in the study.

For all the materials considered the plane wave cutoff energy of 520 eV has been chosen to maintain high accuracy of the total energy calculations. The lattice parameters and internal positions of atoms were fully optimized during the double relaxation procedure employed, and consequently, the minima of the total energies with respect to the lattice parameters and internal ionic positions have been determined. This geometry optimization was obtained by minimizing the Hellman–Feynman forces via a conjugate gradient method, so that the net forces applied on every ion in the lattice are close to zero. The total electronic energies were converged within 10^{-5} eV unit cell^{-1} resulting in the residual force components on each atom to be lower than 0.01 eV Å^{-1} atom^{-1}, thus allowing for the accurate determination of the internal structural parameters. Since the doped structures contain a small amount of additional elements, it is expected that the equilibrium volume of the basic unit cell is not substantially altered. Hence, only internal atomic positions have been optimized during our calculations keeping the volumes of the unit cells identical to that of the corresponding undoped parent materials.

The Monkhorst–Pack scheme was used to sample the Brillouin Zone (BZ) and generate the *k*-point grid for the solids and the different isolated atoms used in the present study. A choice of the appropriate number of *k*-points in the irreducible part of the BZ was based on convergence of the total energy to be 0.1 meV atom^{-1}. For pure and doped forms of $CaTa_2O_6$, $CaNb_2O_6$, as well as for $Ca_2Ta_2O_7$ and $Ca_2Nb_2O_7$, the following numbers of *k*-points in the irreducible parts of BZ were used: 84, 84, 39, and 39 points, respectively. For the total energy calculations of isolated atoms of all elements comprising the materials considered, a cubic box with edges of 10 Å × 10 Å × 10 Å was chosen to eliminate possible interaction between atoms caused by the periodic boundary conditions. Test calculations with the box size of 15 Å × 15 Å × 15 Å for an isolated oxygen atom have shown a difference in total energies within 0.2 meV atom^{-1} with respect to the box size of 10 Å × 10 Å × 10 Å, which is small enough not to contribute a significant error in the calculations of the cohesive energy. Thus, 10 Å × 10 Å × 10 Å box size has been used for all the other elements.

Table 1
Experimental and calculated structural parameters for the undoped compounds. Calculated parameters are shown in parenthesis.

		$CaNb_2O_6$ from [29]	$CaTa_2O_6$ from [30]	$Ca_2Nb_2O_7$ from [31]	$Ca_2Ta_2O_7$ from [31]
a (Å)		14.926 (15.069)	11.068 (11.144)	10.444 (10.315)	10.463 (10.339)
b (Å)		5.752 (5.811)	7.505 (7.557)	–	–
c (Å)		5.204 (5.246)	5.378 (5.394)	–	–
V_0 (Å^3)		446.8 (459.4)	446.7 (454.2)	1139.2 (1097.5)	1145.4 (1105.2)
Z		4	4	8	8
Space group		*Pbcn*; #60 Orthorhombic	*Pnma*; #62 Orthorhombic	*Fd-3m*; #227 Pyrochlore cubic	Fd-3m; #227 Pyrochlore cubic
	x	0	0.042	0.5	0.5
Ca	y	0.2244	0.25	0.5	0.5
	z	0.75	0.540	0.5	0.5
	x	0.1653	0.1412	0	0
Nb or Ta	y	0.3166	−0.0056	0	0
	z	0.2987	0.0376	0	0
	x	0.0893	−0.024	0.3214	0.3214
O_1	y	0.0997	0.035	0.125	0.125
	z	0.4040	0.225	0.125	0.125
	x	0.1003	0.213	0.375	0.375
O_2	y	0.4280	0.049	0.375	0.375
	z	0.0056	0.383	0.375	0.375
	x	0.2576	0.146		
O_3	y	0.1351	0.25	–	–
	z	0.1266	−0.033		
	x		0.122		
O_4	y		−0.25	–	–
	z		0.162		

$CaNb_2O_6$ and $CaTa_2O_6$ adopt orthorhombic crystal structures with *Pbcn* and *Pnma* space groups, respectively, and 36 atoms in the conventional unit cell ($Z = 4$) [29,30]. $Ca_2Nb_2O_7$ and $Ca_2Ta_2O_7$ exhibit the same pyrochlore type of structure with *Fd-3m* space group and $Z = 8$ (88 atom unit cell^{-1}) [31]. It is important that all the structures considered be optimized during the total energy calculations and hence, this spatial atomic distribution can be considered to be a very reasonable initial configuration for conducting further numerical optimization studies.

3. Results and discussion

The electronic structures of orthorhombic $CaNb_2O_6$ and $CaTa_2O_6$ are very close due to the isoelectronic similarity of Nb and Ta. It is also for this reason that $Ca_2Nb_2O_7$ and $Ca_2Ta_2O_7$ with the pyrochlore structure exhibit similar characteristics. Table 1 shows the structural parameters of the oxides obtained experimentally and from our calculations. One can see that the results of the calculations obtained from the structural optimization are in very good agreement with experimental measurements and are characterized by an error of less than 1.0% for orthorhombic structures and ~1.2% for pyrochlore compounds. This margin of error is common for calculations utilizing the GGA approximation for the exchange-correlation potential.

Figs. 1 and 2 show the total density of electronic state (DOS) and partial density of electronic state (PDOS) for all the four parent materials. The energy scale has been shifted in such a way that the zero corresponds to the Fermi energy. The occupied bands of all the materials consist of Ca3p, O2s, O2p, and, to some extent, Nb or Ta d-orbitals. The valence band consists primarily of O2p states with small admixture of transition metal d-orbitals. The conduction bands of the materials are composed of Nb4d or Ta5d orbitals hybridized with another part of O2p states. All of the materials demonstrate a forbidden energy gap between the valence and conduction bands. Values of the band gaps (BGs) calculated within the DFT methodology are usually underestimated, so that the absolute calculated values of BGs should not be taken into quantitative consideration. Electronic structure calculations for these oxides reported in the literature [19,32] demonstrate the same features as discussed above thus validating data obtained in the present study.

Since all the four oxides are semiconductors, their electronic conductivity is still inadequate for use as electrode materials for electrolysis and needs to be improved further to enhance the charge transfer characteristics critical for lowering the over potential and attaining good catalytic activity. As mentioned earlier in Section 1, the electronic conductivity could be improved by adding a small amount of additional elements possessing more valence electrons than Ca or Nb/Ta. Hence these elements will be capable of serving as donors of free charge carriers, thus increasing the electronic conductivity.

Since the goal of the current study is to unravel the principal role of the small concentrations of dopants and their corresponding influence on the electronic conductivity and structural/chemical stability, only one atom of each dopant has been placed into the elementary cell (pyrochlore structure doped with fluorine was the only exception, where two oxygen atoms out of 56 in the unit cell were replaced by fluorine atoms). Such a selection eliminates any uncertainty in the atomic configurations occurring due to the presence of multiple (two or more) doping atoms in the unit cell. For example, the 36 atom elementary unit cell of the orthorhombic $Ca(Nb/Ta)_2O_6$ contains 4 Ca, 8 Nb or Ta, and 24 O ions, so that those elements substituting for Ca in the unit cell will replace one Ca atom out of the four available. Similarly, only one atom from the 6A-group will be substituted for one atom of Nb or Ta out of the existing 8 sites and one atom of F will replace one out of 24 oxygen atoms available in the unit cell. In the case of the pyrochlore structure the 88 atomic elementary unit cell contains 16 Ca atoms, 16 Nb or Ta atoms and 56 O. Again, only one atom of each dopant substitutes for the corresponding atomic site of Ca, Nb, or Ta out of the 16 available for each site, but as mentioned above, two F atoms will replace two oxygen atoms out of 56 available to maintain a reasonable F-concentration in the materials. The valence electronic

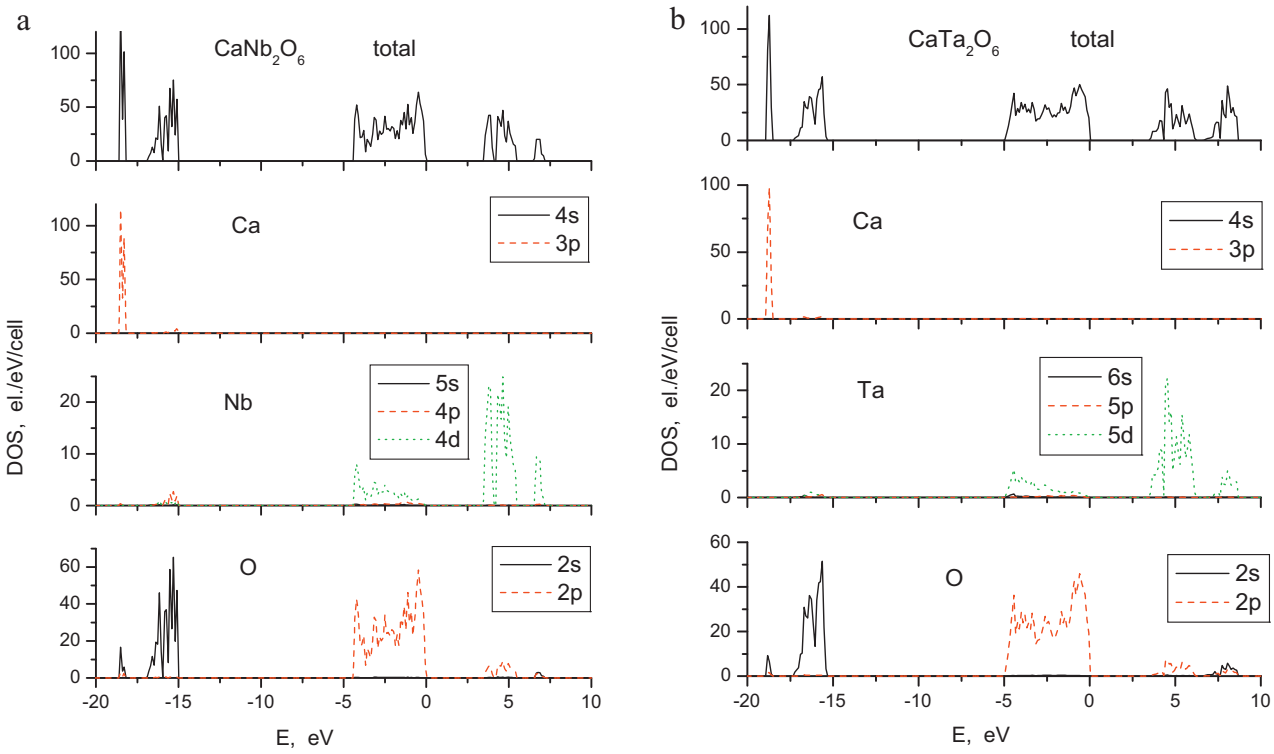

Fig. 1. Electronic density of states for (a) pure $CaNb_2O_6$ and (b) pure $CaTa_2O_6$.

configurations of Ca, Nb, Ta, and O atoms are $4s^23p^6$, $4p^65s^14d^4$, $6s^25d^3$, and $2s^22p^4$, respectively. The electronic configurations for Sc, Y are $4s^23d^1$, $4s^24p^65s^24d^1$, respectively; for B, Al, Ga, In are $2s^22p^1$, $3s^23p^1$, $3d^{10}4s^24p^1$, $4d^{10}5s^25p^1$, respectively; for As, Sb, Bi are $4s^24p^3$, $5s^25p^3$, $6s^26p^3$, respectively; for Cr, Mo, W are $3d^54s^1$, $4d^55s^1$, $5d^46s^2$, respectively; for F – $2s^22p^5$.

Since, the niobates and tantalates considered in the present study have similar electronic structure (compare Figs. 1 and 2) the main discussion of the results in the manuscript primarily focuses on calcium niobates doped with the different elements mentioned above. Most of the conclusions derived from the present study on doped calcium niobates can also be applied to the corresponding

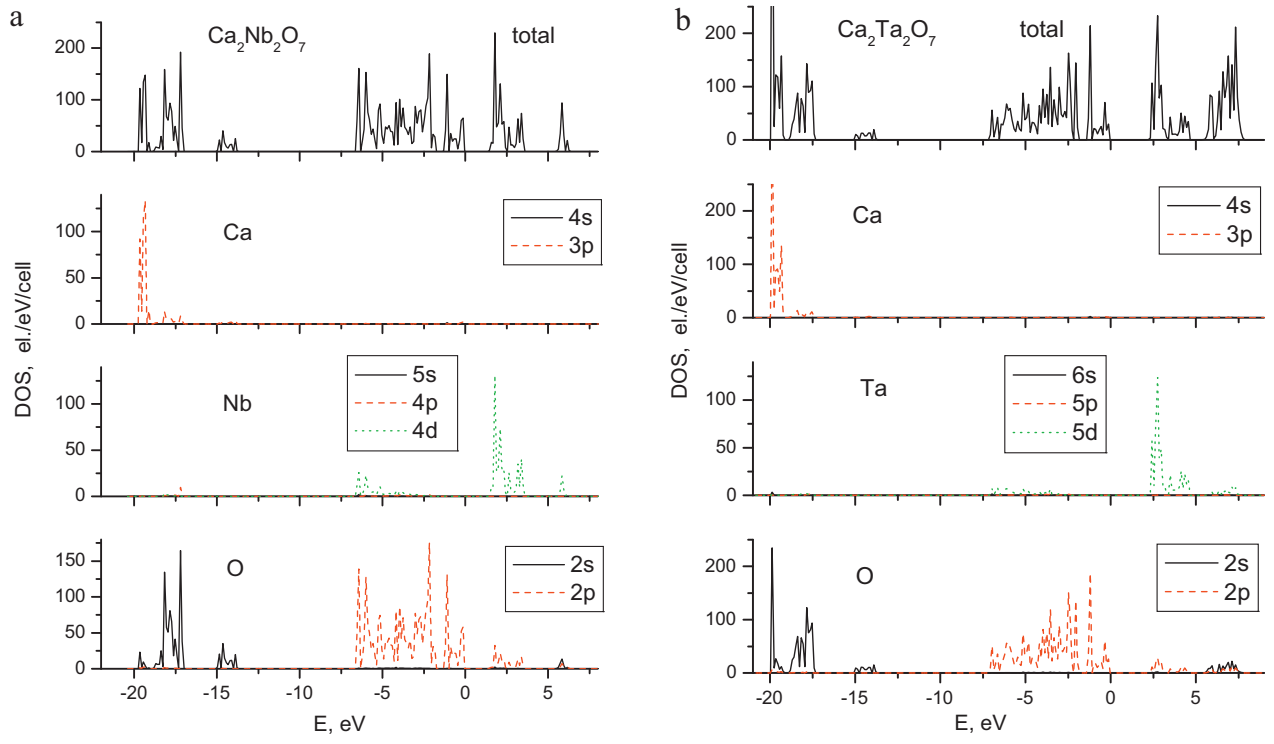

Fig. 2. Electronic density of states for (a) pure $Ca_2Nb_2O_7$ and (b) pure $Ca_2Ta_2O_7$.

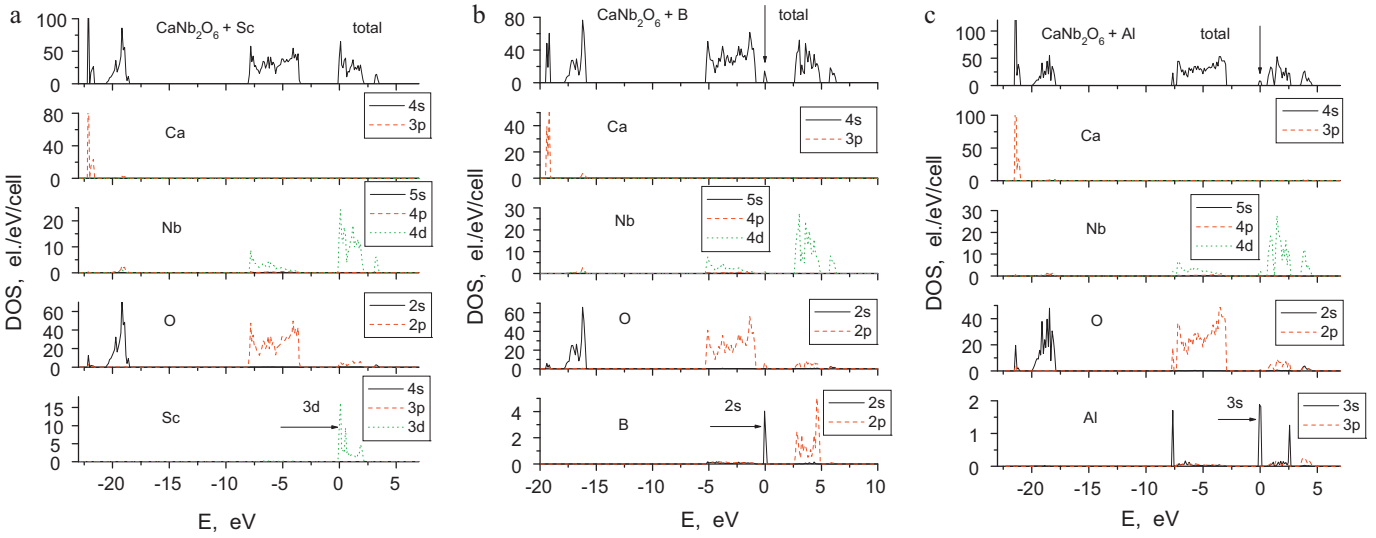

Fig. 3. Electronic density of states for $CaNb_2O_6$ doped with (a) Sc; (b) B; (c) Al.

iso-electronic calcium tantalates, and hence the results obtained for calcium tantalates will be shown mainly for illustration purposes.

3.1. $Ca(Nb/Ta)_2O_6$ with dopants

Due to the isoelectronic nature of elements belonging to the same group of the Periodic Table the electronic structure changes resulted from doping of such elements qualitatively are very similar, so that we will discuss in detail only one or two representative dopants from each group and mention briefly the results for other members of the particular periodic group.

3.1.1. 3A and 3B group elements

As it was mentioned above, we chose Sc and Y from 3A group and B, Al, Ga, and In from 3B. All the elements have valence +3, so that they may serve as donors of additional free electrons when replaced for divalent Ca^{2+}. The total and partial electronic densities of states calculated for $Ca_{0.75}Sc_{0.25}Nb_2O_6$ are shown in Fig. 3a. Almost identical results have been obtained for Y-doping due to the same outer electronic configuration. One can see, that the doped system demonstrates very similar electronic structure as undoped $CaNb_2O_6$ oxide (compare Figs. 1a and 3a). The only prominent difference is that in the doped system the Fermi level shifted towards conduction band making this material metallically conductive. It occurs due to strong hybridization of Sc 3d (or Y 4d) and Nb 4d zones forming the conduction band occupied with additional electrons being brought into the system by the donor serving Sc- or Y-doping. It is worth mentioning that the band gap value between valence and conduction bands is not changed during doping and remains ~3.4 eV. Sc- and Y-doping of $CaTa_2O_6$ demonstrate the same results as for $CaNb_2O_6$ discussed above.

As for doping with 3B-elements, the results are much more different from those seen for 3A-dopants. The total and partial DOS for $CaNb_2O_6$ doped with B and Al are shown in Fig. 3b and c. In contrast to doping of 3A-elements, incorporation of 3B-elements introduces a new non-hybridized completely localized impurity zone which is their own valence s-states located in the energy gap between valence and conduction bands (see partial density of states of B and Al in the bottom graphs in Fig. 3b and c and denoted by arrows). This impurity s-zone is separated from the main conduction band by an energy gap of 2.42 eV for B and 0.44 eV for Al doping, which is the value of the activation energy, E_a for the electronic conductivity determined by electron transitions from these localized s-states to the conduction band. Quite similar situations are observed for Ga- and In-doped $CaNb_2O_6$ and $CaTa_2O_6$. The corresponding activation energy values E_a together with resulting types of conductivity are collected in Table 2a for all the materials considered in the present study.

3.1.2. 5B and 6A group elements and F

The total and partial DOS calculated for $Ca_{0.75}As_{0.25}Nb_2O_6$, $Ca[Nb_{0.875}Cr_{0.125}]_2O_6$ and $Ca[Nb_{0.875}W_{0.125}]_2O_6$ are shown in Fig. 4a–c. In contrast to pure $CaNb_2O_6$, the electronic structures of the doped oxides display several features related to the substituted dopants. The main differences between pure $CaNb_2O_6$ and the structure doped with As, Sb, or Bi (Sb and Bi doped compounds are not shown due to their similarity) are the appearance of the s-states of the dopants indicated by arrows hybridized with O2p states located at the bottom of the valence band and separated from the upper portion of the valence band by an energy gap of 3–4.5 eV (see Fig. 4a). Also, similar to 3A dopants due to additional free electrons brought into the system, the Fermi level of the doped structures also is shifted towards the conduction band resulting in metallic conductivity of the material. The band gap between the valence and conduction bands is about 3.2 eV and does not change significantly with respect to that of the undoped oxide (3.4 eV), so that small amounts of 5B-group elements do not noticeably affect the width of the forbidden zone. A similar picture is observed for $CaTa_2O_6$ doped with the same 5B elements demonstrating that the values of the energy gap between the valence and conduction bands for all the three dopants are 3.10 eV, 3.15 eV and 3.40 eV for As, Sb and Bi, respectively, which correlates well with the calculated band gap for the pure $CaTa_2O_6$ of ~3.4 eV.

Incorporation of 6A transition metal, such as Cr, Mo, and W demonstrates similar features in the electronic structure as those resulting due to 3B-doping (see Fig. 4b and c). Cr, Mo and W as dopants introduce new states which are their own valence d-states located in the energy gap between valence and conduction bands and marked with arrows in Fig. 4b and c. In case of $Ca[Nb_{0.875}Cr_{0.125}]_2O_6$ the partially occupied Cr3d-states are completely localized and separated from the main conduction band by an energy gap of about 1.76 eV. Quite a similar situation is observed for Mo-doped $CaNb_2O_6$. There is also a partially occupied middle portion of Mo4d-states separated from the upper conduction band by a small energy gap of ~0.22 eV that facilitates electron transition to the conduction band and, thus improves the overall electronic

Table 2a
Cohesive energy (eV f.un.$^{-1}$ and eV atom^{-1}), band gap (BG), band gap values between electronic states located at Fermi level and the main conduction band and type of conductivity calculated for undoped oxides and doped with 3A and 3B group elements. Experimental BG for pure oxides is taken from: [32] for $CaNb_2O_6$, [19] for $Ca_2Nb_2O_7$ and $Ca_2Ta_2O_7$, [20] for $CaTa_2O_6$.

	Pure	Periodic group					
		3A		3B			
		Sc	Y	B	Al	Ga	In
$CaNb_2O_6$							
$-E_{coh}$ (eV f.un.$^{-1}$)	61.92	62.164	62.49	60.146	61.01	60.65	60.68
$-E_{coh}$ (eV atom^{-1})	6.88	6.91	6.94	6.68	6.78	6.74	6.742
BG (eV)	3.413	0	0	2.42	0.44	1.1	0.44
Conductivity	3.87exp	met	met	semi	semi	semi	semi
$Ca_2Nb_2O_7$							
$-E_{coh}$ (eV f.un.$^{-1}$)	73.105	73.34	73.49	72.36	72.74	72.57	72.58
$-E_{coh}$ (eV atom^{-1})	6.65	6.67	6.68	6.58	6.61	6.60	6.60
BG (eV)	1.28	0	0	1.1	0	0.33	0
Conductivity	2.95exp	met	met	semi	met	semi	met
$CaTa_2O_6$							
$-E_{coh}$ (eV f.un.$^{-1}$)	66.77	66.89	67.26	64.89	65.724	65.41	65.46
$-E_{coh}$ (eV atom^{-1})	7.42	7.43	7.47	7.21	7.30	7.27	7.273
BG (eV)	3.414	0	0	2.75	0.33	1.43	0.33
Conductivity	4.0exp	met	met	semi	semi	semi	semi
$Ca_2Ta_2O_7$							
$-E_{coh}$ (eV f.un.$^{-1}$)	78.146	78.30	78.43	77.41	77.76	77.60	77.60
$-E_{coh}$ (eV atom^{-1})	7.10	7.12	7.13	7.04	7.07	7.05	7.05
BG (eV)	2.133	0	0	1.9	0.11	0.77	>0.1
Conductivity	3.58exp	met	met	semi	semi	semi	semi

conductivity of the material. Finally, in the case of the W-doped material these corresponding W5d-states overlap with the Nb5d conduction band thus resulting in the activation energy for the conductivity equal to zero (Fig. 4c). In the case of $CaTa_2O_6$ doped with Cr, Mo, and W, all three doped oxides remain semiconductors and there is no overlap between W5d-states and the Ta5d conduction band (see Table 2b) for the activated conductivity values.

Fig. 5 shows DOS calculated for F-doped $CaNb_2O_6$. As expected, F introduces its own local p-zone located ~2 eV below the main valence zone formed by 2p-states of oxygen. Total density of states in the vicinity of the Fermi level is very similar to what one can see in the case of the structure doped with group 3A (Sc) and group 5B (As) elements. No impurity states appear within the band gap so that the Fermi level shifts towards the conduction band resulting in metallic conductivity of the material. The same result is observed for F-doped $CaTa_2O_6$ as well as for fluorine doped tin oxide (SnO_2:F) systematically investigated and reported by us recently in [24].

3.2. *Pyrochlore $Ca_2(Nb/Ta)_2O_7$ with dopants*

It should be noted that the pyrochlore niobates and tantalates doped with all the dopants considered here demonstrate very similar behavior in terms of band structure in the vicinity of the Fermi level and activated conductivity as for corresponding doped orthorhombic structure of $Ca(Nb/Ta)_2O_6$.

Fig. 6a–c demonstrates the electronic density of states calculated for the pyrochlore structures of calcium niobates doped with Sc, B, and Al, respectively. The pyrochlore niobate doped with Sc (as well as with Y) do not demonstrate significant changes in their electronic structure with respect to the pure undoped structure

Table 2b
Cohesive energy (eV f.un.$^{-1}$ and eV atom^{-1}), band gap (BG), band gap values between electronic states located at Fermi level and the main conduction band and type of conductivity calculated for oxides doped with 5B, 6A and 7B group elements.

	Periodic group						
	5B			6A			7B
	As	Sb	Bi	Cr	Mo	W	F
$CaNb_2O_6$							
$-E_{coh}$ (eV f.un.$^{-1}$)	60.17	60.45	60.53	59.94	60.95	61.61	61.08
$-E_{coh}$ (eV atom^{-1})	6.658	6.72	6.725	6.66	6.77	6.85	6.79
BG (eV)	0	0	0	1.76	0.22	0	0
Conductivity	met	met	met	semi	semi	met	met
$Ca_2Nb_2O_7$							
$-E_{coh}$ (eV f.un.$^{-1}$)	72.38	72.51	72.53	72.19	72.64	73.0	72.59
$-E_{coh}$ (eV atom^{-1})	6.58	6.59	6.593	6.56	6.60	6.64	6.60
BG (eV)	0	0	0	1.32	0.33	0.15	0
Conductivity	met	met	met	semi	semi	semi	met
$CaTa_2O_6$							
$-E_{coh}$ (eV f.un.$^{-1}$)	64.93	65.195	65.32	64.16	65.67	65.88	65.83
$-E_{coh}$ (eV atom^{-1})	7.214	7.24	7.26	7.13	7.30	7.32	7.31
BG (eV)	0	0	0	1.21	0.77	0.22	0
Conductivity	met	met	met	semi	semi	semi	met
$Ca_2Ta_2O_7$							
$-E_{coh}$ (eV f.un.$^{-1}$)	77.38	77.45	77.46	76.94	77.35	77.70	77.41
$-E_{coh}$ (eV atom^{-1})	7.03	7.04	7.04	6.99	7.03	7.06	7.037
BG (eV)	0.2	0	0	2.2	1.1	0.53	0
Conductivity	semi	met	met	semi	semi	semi	met

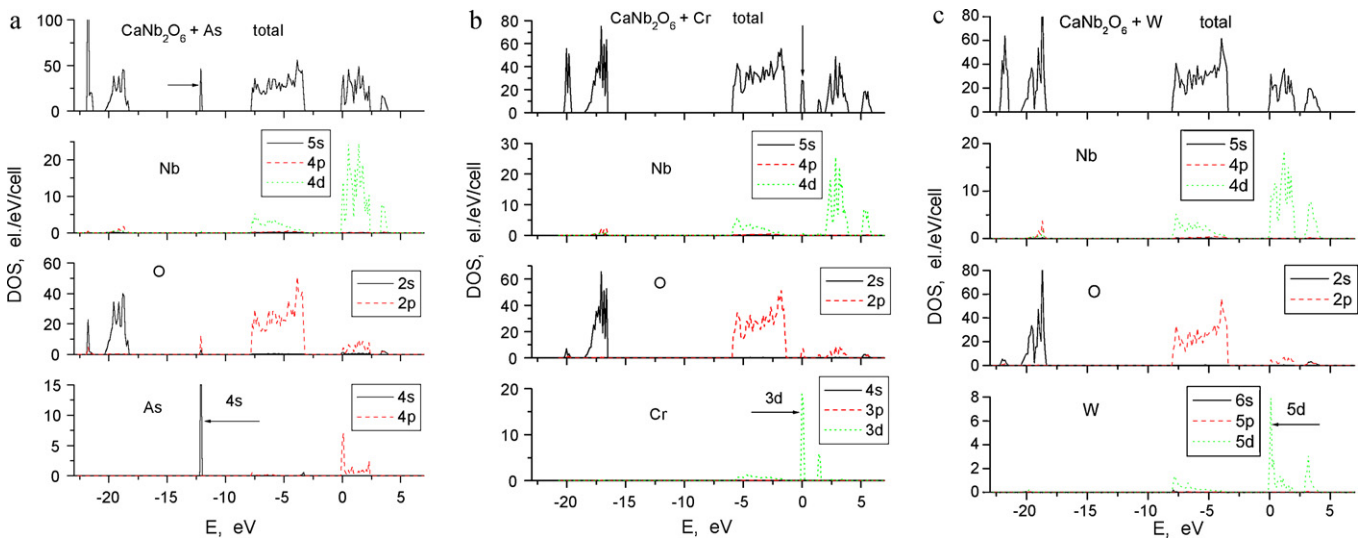

Fig. 4. Electronic density of states for $CaNb_2O_6$ doped with (a) As; (b) Cr; (c) W.

(compare Figs. 2a and 6a). The only distinction noticeably evident is the Fermi level located at the bottom of the conduction band, since an additional valence electron has been contributed into the whole system by the impurity atom. Thus the d-states of the dopants are located at the same energy level as the Nb4d resulting in the states being hybridized with each other. Thus, similar to $Ca(Nb/Ta)_2O_6$ doping with Sc and Y of pyrochlore niobates and tantalates renders these compounds also metallic.

As for the pyrochlore niobates doped with 3B (B, Al, Ga, In) elements, there is an impurity zone that appears within the forbidden energy gap of the pure oxide arising from the partially occupied s-states of the doping elements (Fig. 6b). The band gap between these local states and the upper part of the conduction band varies depending on the dopant. For B and Ga the gap is 1.1 and 0.33 eV, respectively, although for Al and In these valence s-bands overlap with conduction Nb4d-zone eliminating the gap completely (see Fig. 6c). However, pyrochlore tantalate doped with Al and In remains still semiconductor although with very small band gap of ~0.1 eV. In fact, doping the structure with all group 3B elements renders the tantalate semiconducting as summarized in Table 2a.

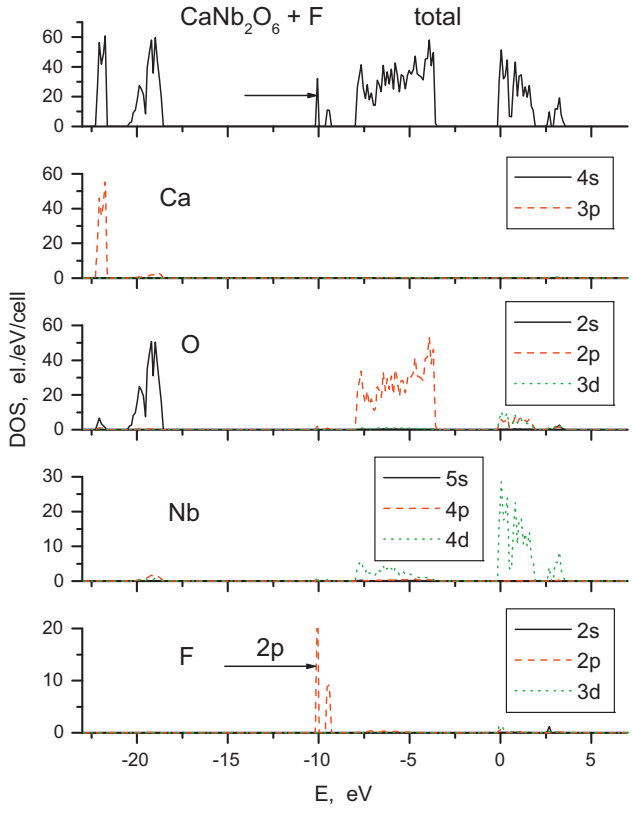

Fig. 5. Electronic density of states for $CaNb_2O_6$ doped with F.

The pyrochlore niobates and tantalates doped with 6A and 5B elements as well as F demonstrate almost identical behavior in terms of electronic conductivity corresponding to doped $CaNb_2O_6$ and $CaTa_2O_6$. The only exception is As-doped $Ca_2Ta_2O_7$ demonstrating semiconductor behavior with E_a ~0.2 eV in contrast to all other oxides doped with 6A elements showing metallic behavior. Also, both W-doped $Ca_2Nb_2O_7$ and $Ca_2Ta_2O_7$ are semiconductors in contrast to W-doped $CaNb_2O_6$ when W5d-states overlap with Nb4d-states rendering metallic conductivity of the material.

Thus, based on the results obtained on the electronic structure peculiarities demonstrated due to introduction of the small amount of different elements from 3A, 3B, 5B, 6A, and 7B periodic groups one can make a conclusion, that all the dopants do improve the electronic conductivity of all the calcium niobates and tantalates, although to different extents. According to the energy values collected in Tables 2a and 2b one can see that the presence of 3A-, 5B-, and 7B-dopants helps improve the electronic conductivity much better than those containing 3B- and 6A-elements as dopants. The compounds doped with Sc, Y, As, Sb, Bi, and F demonstrate a metal-type conductivity, while those doped with B, Al, Ga, In, Cr, Mo, and W are characterized by the semiconductor type of conductivity (except W-doped $CaNb_2O_6$ and Al- and In-doped $Ca_2Nb_2O_7$, resulting most likely due to above mentioned band gap underestimation typical for DFT methodology).

3.3. Structural and chemical stability

Cohesive energy E_{coh} can be considered as a measure of an overall structural and chemical stability of the material. A higher E_{coh} would therefore imply that more energy is required to break the primary chemical bonds of the compound during chemical reaction or mechanical loading. The present study is dedicated to the identification of the most electrochemically stable materials that can likely withstand the water electrolysis conditions when

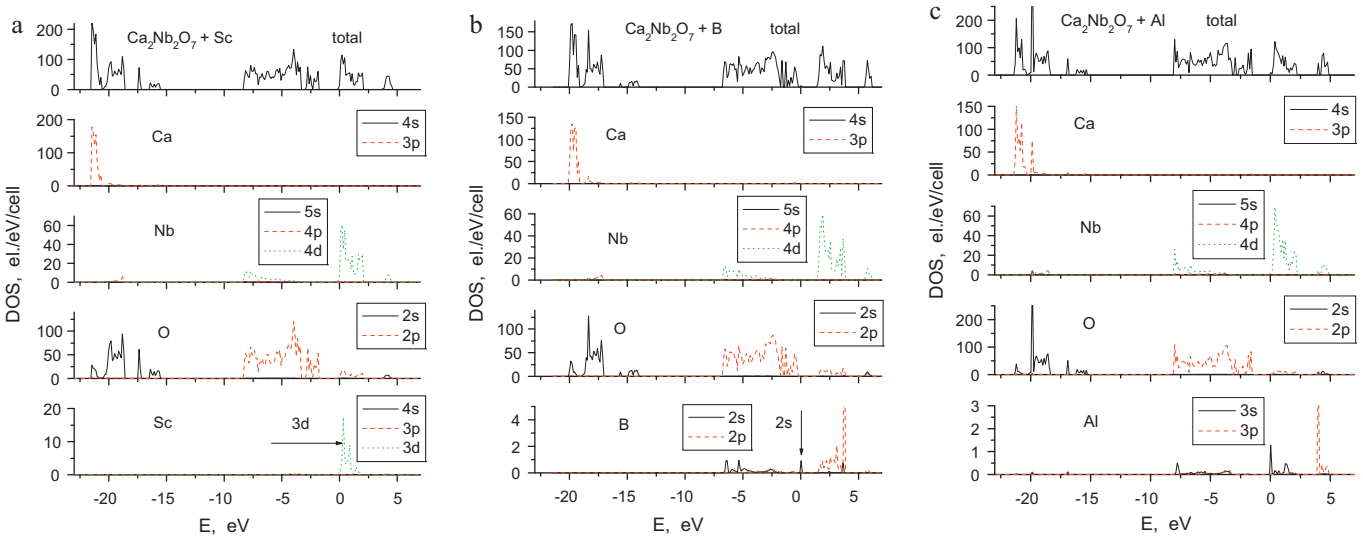

Fig. 6. Electronic density of states for $Ca_2Nb_2O_7$ doped with (a) Sc; (b) B; (c) Al.

exposed to acidic or other aggressive environments. Mechanical strength is thus not one of the main requirements for identification of a promising catalyst support material. Hence, chemical stability in contrast to the ability of the material to sustain high mechanical loading will be the main quantity characterized by the cohesive energy in the present study. Since, Nb and Ta are iso-electronic, we assume that all the four compounds will likely exhibit similar chemistries, but different chemical reactivity when exposed to acidic or other aggressive environments. The value of the cohesive energy E_{coh}, thus could serve as a qualitative criterion for comparing and selecting materials that would likely exhibit the most resistance to decomposition when exposed to chemically reactive environments of aggressive acids and bases.

Since the current work relates to predicted use of promising systems for water electrolysis supports, it is germane to discuss the accuracy of the calculations. In regards to the accuracy of the calculated cohesive energies within the density functional theory utilized in the present study in general, an error of less than 10% is considered to be normal and depends on various parameters involved in the computational model, which might seem to be unacceptably large for fulfilling the objectives for each system investigated in the present study. However, the relative differences in cohesive energies calculated for the different compounds within the same computational approach are expected to be accurate, and sufficient for the qualitative comparison of the electrochemical stability between the materials considered. This qualitative comparison is deemed sufficient to determine the usefulness of the system for exploring as supports for electrocatalysis and water electrolysis.

Calculated cohesive energies for the pure and all the doped oxide structures considered in the present study are collected in Tables 2a and 2b and shown in Fig. 7 for illustrative purposes. One can see that all the structurally analogous tantalate compounds have higher absolute values of cohesive energy than their corresponding niobium analogs and thus, are more stable. It occurs due to the stronger Ta–O interactions in comparison with the Nb–O bonds in the (Ta/Nb)–O_6 octahedra. A comparison of the compounds in terms of the cohesive energy values calculated per atom (not per formula unit) is conceivably incorrect particularly due to the different amounts of atoms per formula unit (9 atoms for $Ca(Nb/Ta)_2O_6$ and 11 atoms for $Ca_2(Nb/Ta)_2O_7$) in the case of the materials considered in this study. However, it may help provide some qualitative explanations for the high mechanical and chemical stability of the materials considered. Hence, we have resorted to comparing the chemical stability of the various pure and doped systems using the cohesive energy calculated per atom. Based on the calculated values of cohesive energy per atom shown in Table 2a and Fig. 7, the structural stability of the materials increases as follows: $Ca_2Nb_2O_7$ (-6.65 eV atom^{-1}) < $CaNb_2O_6$ (-6.88 eV atom^{-1}) < $Ca_2Ta_2O_7$ (-7.10 eV atom^{-1}) < $CaTa_2O_6$ (-7.42 eV atom^{-1}). Also, it can be clearly seen that basically introduction of all dopants make these compounds less stable, although to different extents. The only exception is the doping of 3A group elements which renders all the four parent oxides even more stable. This directly relates with the Sc–O and Y–O bonds which are stronger than the Ca–O bonds in the corresponding parent compounds. All other dopant elements decrease the structural and chemical stability, although all the doped compounds are more stable than pure SnO_2 or SnO_2 doped with fluorine used as catalyst support material for water electrolysis (calculated E_{coh} for pure SnO_2 is -5.08 eV atom^{-1} and for SnO_2 doped with ~6.2 wt% of F is -4.74 eV atom^{-1}) [24].

Thus, based on the previous discussion it allows us to conclude that in terms of general stability, the orthorhombic $CaTa_2O_6$ with a cohesive energy of -7.42 eV atom^{-1} can be marked as the most stable compound among the entire four parent oxides considered

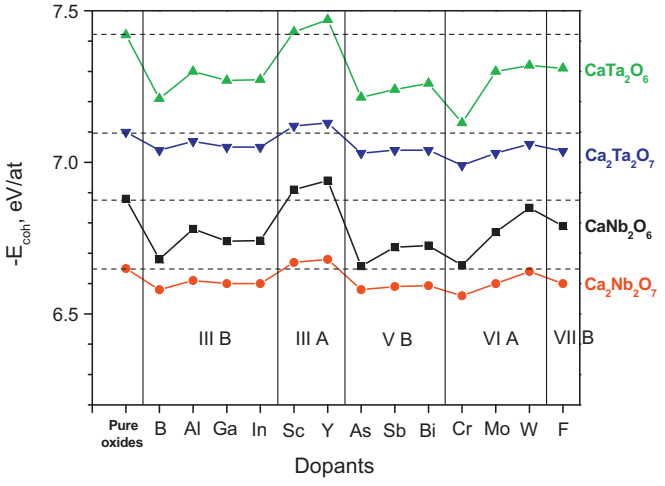

Fig. 7. Cohesive energy $-E_{coh}$ for all the materials in eV atom^{-1}.

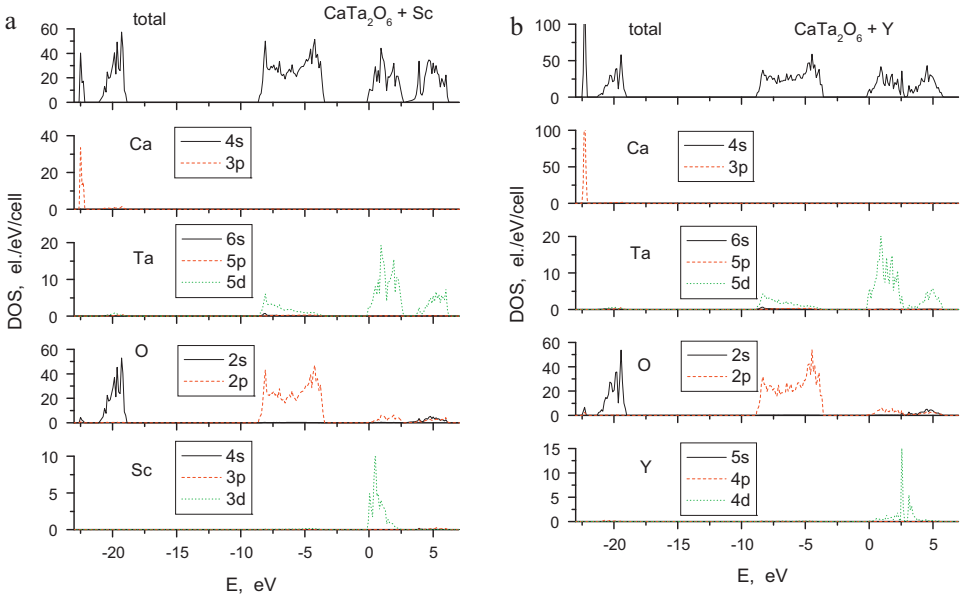

Fig. 8. Electronic density of states for $CaTa_2O_6$ doped with (a) Sc; (b) Y.

in the present study. However, $CaTa_2O_6$ doped with Sc and Y render the oxide even more stable with $E_{coh} = -7.43$ and -7.47 eV atom^{-1}, respectively. It is also noteworthy to mention that among all the calcium tantalates considered in the study the least stable is $Ca_2Ta_2O_7$ doped by Cr with $E_{coh} = -6.99$ eV atom^{-1}. However, it demonstrates a higher stability in comparison to the most stable niobate $CaNb_2O_6$ doped with Y indicating a $E_{coh} = -6.94$ eV atom^{-1}. Hence, it could be construed that the tantalate-based compounds are more resistant to decomposition and cleavage of the primary bonds when exposed to harsh mechanical or chemical environments such as those likely experienced by these systems when used in highly corrosive acidic environments. Hence it can be expected that these tantalate based compounds could function well when used as electro-catalyst supports in electrochemical systems comprising water electrolysis and the oxygen reduction reactions (ORR) in proton exchange membrane based fuel cells.

As for the electronic conductivity, due to an increased charge carrier density in the presence of additional dopants all the four doped niobates and tantalates are expected to demonstrate better conductivity in comparison to the pure undoped parent oxides. Doping the oxides with 3B and 6A elements result in lowering the activated conductivity E_a in comparison to undoped materials, although the compounds remain semiconductors. Moreover, all four niobates and tantalates doped with 3A, 5B (with the exception of As doped $Ca_2Ta_2O_7$) and 7B elements demonstrate metallic type of conductivity with zero activation energy. Among them, as we mentioned above, $CaTa_2O_6$ doped with Sc and Y (3A group) demonstrate the highest values of cohesive energy, metallic conductivity, and excellent structural and chemical stability. Thus these systems could be considered as the most appropriate candidates for the catalyst support in PEM based electrolysis.

For illustrative purposes the calculated DOS for Sc and Y-doped $CaTa_2O_6$ are shown in Fig. 8. Also, Table 3 includes a list of weight percentages of Sc and Y used as dopants for all the four parent oxides considered in the present study.

Table 3
Concentrations of Sc and Y in all cases considered in present study.

	Sc (wt%)	Y (wt%)
$CaNb_2O_6$	3.48	6.66
$Ca_2Nb_2O_7$	1.48	2.90
$CaTa_2O_6$	2.25	4.36
$Ca_2Ta_2O_7$	1.01	1.99

4. Conclusions

An attempt to identify new electrochemically stable catalyst supports for electrolysis of water using *ab initio* density functional theory approach has been undertaken in the present study. Calcium niobates $Ca_2Nb_2O_7$, $CaNb_2O_6$ and calcium tantalates $Ca_2Ta_2O_7$, $CaTa_2O_6$, have been chosen to systematically investigate the influence of small amounts of dopants selected from group 3A, 3B, 5B, 6A and 7B of the Periodic Table on the electronic conductivity and structural stability of the compounds. The study showed that small amounts of 3A-, 5B- and 7B-group elements noticeably improve the conductivity than the elements from group 3B and group 6A of the Periodic Table. Also, a comparison of the cohesive energies calculated for the pure and doped oxides displayed $CaTa_2O_6$, and Y doped $CaTa_2O_6$ to be the most stable compound among all materials considered in the study.

The study thus allows us to hypothesize based on electronic conductivity and cohesive energy considerations that the $CaTa_2O_6$ doped with Sc and Y is the most appropriate candidate for use as a catalyst support in water electrolysis. However, this conclusion needs to be verified with further experimental validations. Unfortunately, to the best of our current knowledge, there are no published experimental reports on any measurements of electronic conductivity of calcium niobates or tantalates doped with the dopants considered in the present study. Experimental validation of the calculated predictions reported in this work are currently planned to be conducted in our laboratory which will be reported in subsequent publications.

Acknowledgements

Research supported by the U.S. Department of Energy, Office of Basic Energy Sciences, Division of Materials Sciences and Engineering under Award DE-SC0001531. PNK acknowledges the Edward R. Weidlein Chair Professorship funds and the Center for Complex Engineered Multifunctional Materials (CCEMM) for procuring the electrochemical equipment used in this research work. The authors also thank Dr M.K. Datta for fruitful discussions. Finally, the authors

gratefully acknowledge the support of the Pittsburgh Supercomputing Center for allocated computational units.

References

[1] G.W. Crabtree, M.S. Dressehaus, M.V. Buchanan, Phys. Today 57 (2004) 39–45.
[2] J. Ohi, J. Mater. Res. 20 (2005) 3180–3187.
[3] J.A. Turner, Science 285 (1999) 687–689.
[4] J.M. Ogden, Phys. Today 55 (2002) 69–75.
[5] S. Satyapal, J. Petrovic, C. Read, G. Thomas, G. Ordaz, Catal. Today 120 (2007) 246–256.
[6] S. Yeh, H.D. Loughlin, C. Shay, C. Gage, Proc. IEEE 94 (2006) 1838–1851.
[7] F. Barbir, Solar Energy 78 (2005) 661–669.
[8] F. Barbir, Chem. Ind. Chem. Eng. 11 (2005) 105–113.
[9] S. Trasatti, Electrochim. Acta 45 (2000) 2377–2385.
[10] S. Trasatti, Electrochim. Acta 36 (1991) 225–241.
[11] A.J. Terezo, J. Bisquert, E.C. Pereira, G.G. Belmonte, J. Electroanal. Chem. 508 (2001) 59–69.
[12] G.P. Vercesi, J. Rolewicz, C. Comninellis, J. Hinder, Thermochim. Acta 176 (1991) 31–47.
[13] C. Baruffaldi, S. Cattarin, M. Musiani, Electrochim. Acta 48 (2003) 3991–3998.
[14] O. Velikokhatnyi, P. Kumta, Physica B: Condens. Matter 404 (2009) 1737–1745.
[15] I.G. Ismailzade, Izv. Akad. Nauk SSSR Seriya Fizicheskaya 22 (1958) 1485–1487.
[16] K. Kawajiri, Y. Yamasaki, Y. Sugitani, Nippon Kagaku Kaishi 9 (1978) 1244–1248.
[17] D.R. Lide, H.V. Kehiaian, CRC Handbook of Thermophysical and Thermochemical Data, CRC Press, 1994.
[18] I.S. Cho, S.T. Bae, D.K. Yim, D.W. Kim, K.S. Hong, J. Am. Ceram. Soc. 92 (2009) 506–510.
[19] L. Zhang, H. Fu, C. Zhang, Y. Zhu, J. Phys. Chem. C 112 (2008) 3126–3133.
[20] K. Domen, M. Hara, J.N. Kondo, T. Takata, A. Kudo, H. Kobayashi, Y. Inoue, Korean J. Chem. Eng. 18 (2001) 862–866.
[21] A.V. Moholkar, S.M. Pawar, K.Y. Rajpure, C.H. Bhosale, J.H. Kim, Appl. Surf. Sci. 255 (2009) 9358–9364.
[22] D. Zaouk, R. al Asmar, J. Podelecki, Y. Zaatar, A. Khoury, A. Foucaran, Microelectron. J. 38 (2007) 884–887.
[23] J. Xu, S. Huang, Z. Wang, Solid State Commun. 149 (2009) 527–531.
[24] O. Velikokhatnyi, P. Kumta, Physica B: Condens. Matter 406 (3) (2011) 471–477.
[25] G. Kresse, J. Furthmuller, Phys. Rev. B 54 (1996) 11169–11186.
[26] G. Kresse, J. Furthmuller, Comput. Mater. Sci. 6 (1996) 15–50.
[27] G. Kresse, D. Joubert, Phys. Rev. B 59 (1999) 1758–1775.
[28] J.P. Perdew, Y. Wang, Phys. Rev. B 33 (1986) 8800–8802.
[29] J.P. Cummings, S.H. Simonsen, Am. Mineral. 55 (1–2) (1970) 90–97.
[30] L. Jahnberg, Acta Chem. Scand. 71 (1963) 2548–2559.
[31] J. Lewandowski, I. Pickering, Mater. Res. Bull. 27 (1992) 981–988.
[32] I.-S. Cho, S.T. Bae, D.H. Kim, K.S. Hong, Int. J. Hydrogen Energy 35 (2010) 12954–12960.